Three Papers Concerning the Lockman Hole

Stevie Dunn

The Astrophysical Journal

- All three appear in the Supplement Series,
- Volume 154, 2004 September
- Issue devoted exclusively to the early science achieved with the Spitzer Space Telescope

The Lockman Hole

- column density of galactic hydrogen is minimal
- region well studied in a breadth of wavelengths
- area of 15 square degrees between pointer stars of the big dipper

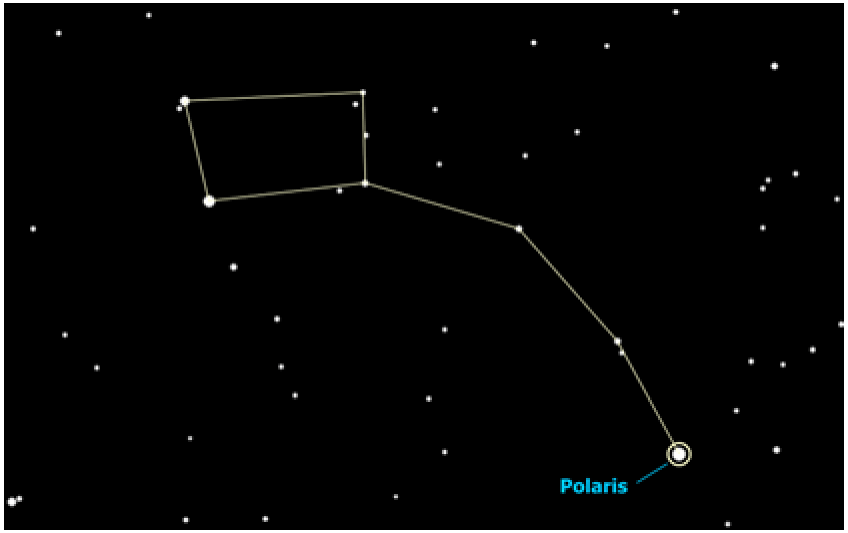

http://www.openzine.com/images/IssueImages/IloadIm

http://www.daviddarling.info/encyclopedia/L/Lockman_Hole.html

First Paper – Basic Information

- Infrared Array Camera (IRAC) Imaging of the Lockman Hole
- J.-S. Huang et al.
- Pages 44-47
- Received 2004 March 26; Accepted 2004 April 29

First Paper - Introduction

- detecting galaxies at high redshifts
- too much dust for optical studies
- efficiency of far-infrared and submillimeter surveys for detecting high-redshift starburst galaxy samples (successful SCUBA surveys for ULIRGs)
- report Spitzer survey results from the IOC period (demonstrate sensitivity for high-redshift galaxy detection)
- both IRAC and MIPS observations of a 4'7 × 4'7 field in the Lockman Hole (second paper focuses on MIPS observation results)

First Paper – Observations and Data Reduction

Number of Objects Detected in the IRAC Bands

Band (μm)	Galaxies	Stars	Total	Magnitude Limit (5 σ, AB)
3.6	419	13	432	23.73
4.5	403	13	413	23.77
5.8	120	5	125	21.90
8.0	80	5	85	21.68
24.0	32	0	32	18.15

- All IRAC bands (3.6, 4.5, 5.8, and 8.0 µm)
- 30 second frame time; 25 dithers per pointing; 670 seconds in each band
- Basic Calibrated Data – Spitzer Science Center (flat-field corrections, dark subtraction, calibrated linearity and flux)
- additional steps: pointing refinement, distortion correction, mosaicking, sigma-clipping to reject cosmic rays
- DAOPHOT source extraction
- discerned stars from galaxies by morphology (Subaru R-band)
- Table 1 – numbers of galaxies and stars detected in each band and the limiting flux

First Paper – Properties of Galaxies Detected by IRAC

- no redshifts available for most of the IRAC sample; color-color diagrams estimate redshifts
- photometric redshift indicator: 1.6 µm bump caused by H^{-} opacity minimum in the atmospheres of cool stars (seen in spectral energy distributions of all galaxies except AGN dominated ones)
- Figures 1 and 2 show the IRAC data and typical SED tracks as a function of redshift
- Figure 1 shows that the observed colors are consistent with the model tracks

First Paper – Properties of Galaxies Detected by IRAC

Figure 1

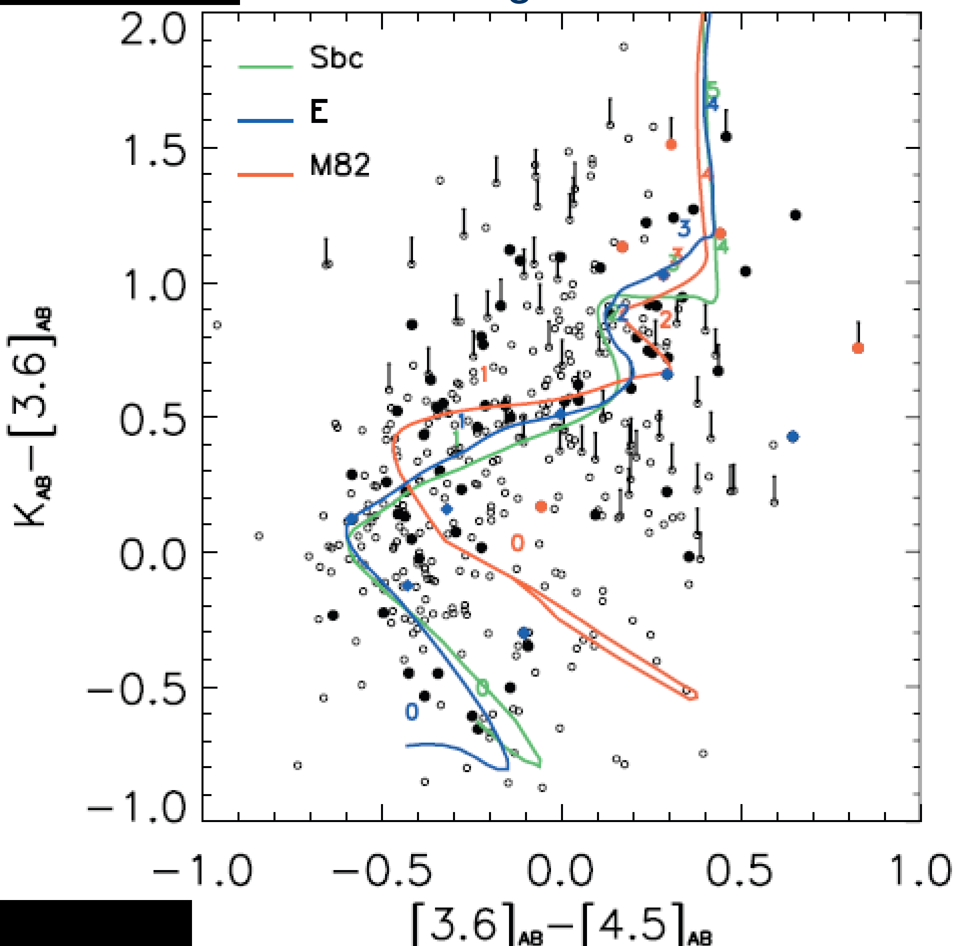

Figure 2

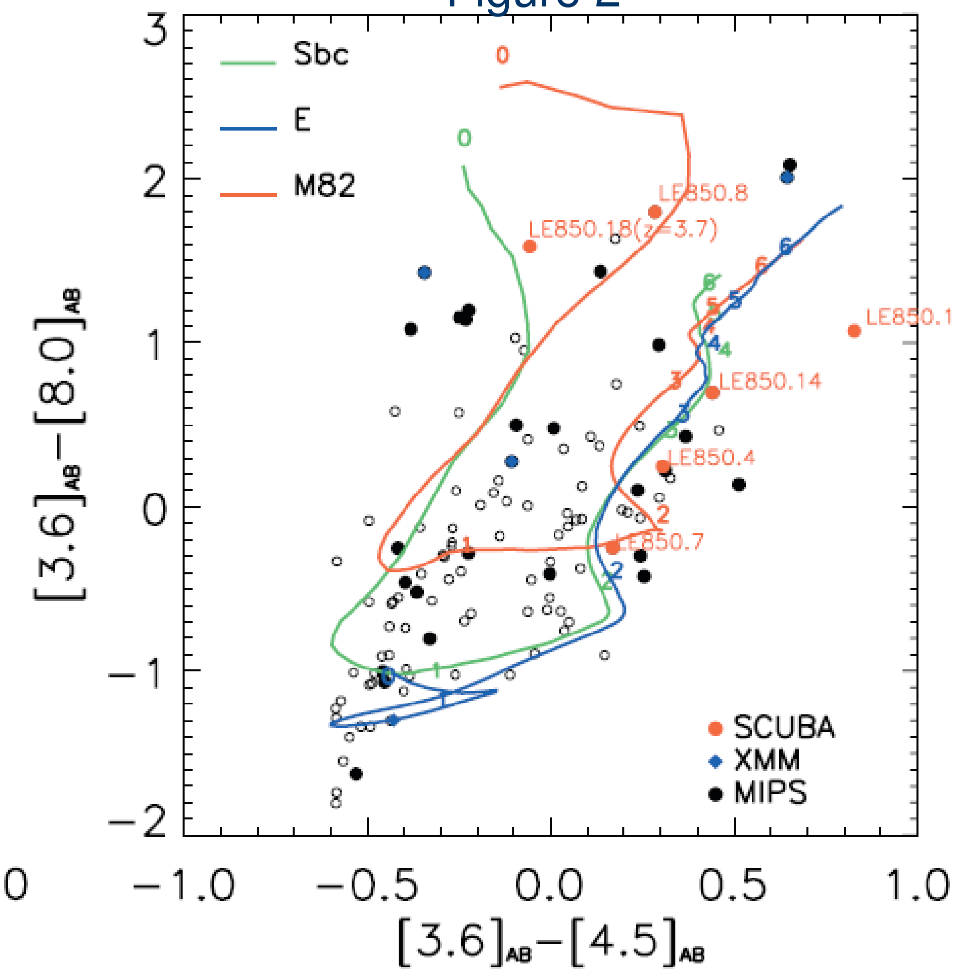

First Paper – Properties of Galaxies Detected by IRAC

- most populated redshift bin for all four IRAC bands is 0.6 < z < 1.3 (50% of all detected IRAC galaxies)
- Paper 2 will give further analysis of how these objects compare with the SCUBA sources
- Table 2 summarizes the observed galaxy number distribution as a function of color (implies redshift)

TABLE 2

GALAXIES IN EACH IRAC COLOR BIN

$K_{AB} - [3.6]_{AB}$	$[3.6]_{AB} - [4.5]_{AB}$	Estimated Redshift	3.6 μm	4.5 μm	5.8 μm	8.0 μm	24 μm
>0	>0	$z > 1.3$	113	122	35	24	16
>0	<0	$0.6 < z < 1.3$	191	176	57	34	8
<0	<0	$z < 0.6$	101	81	27	22	8
<0	>0	$z < 0.6$	14	24	1	0	0

First Paper – Properties of Galaxies Detected by IRAC

- MIPS detected 32 sources in the 24 µm band; the IRAC counterparts show that half of these are at $z > 1.3$ with a minimum infrared luminosity of $10^{12}\ L_{\odot}$ and therefore are **LIRGs and ULIRGs**
- the **extragalactic background light** from extragalactic sources is an indicator of the **total luminosity** of the universe
- the integral resolved galaxy light in a deep survey can give a lower limit on the EBL (since **intermediate redshift galaxy population contributes most to the EBL**)
- Table 3 shows the results of integrating the fluxes from IRAC counterparts of objects identified by SCUBA, XMM-Newton, and MIPS 24 µm images

First Paper – Properties of Galaxies Detected by IRAC

TABLE 3

INTEGRATED GALAXY LIGHT νI_ν (nW m^{-2} sr^{-1}) IN THE IRAC BANDS

Objects	3.6 μm	4.5 μm	5.8 μm	8.0 μm
All galaxies detected.................	3.47	2.43	1.31	1.03
SCUBA counterparts	0.05	0.05	0.05	0.04
XMM-Newton counterparts.......	0.13	0.12	0.13	0.14
MIPS counterparts	0.68	0.52	0.43	0.62

The XMM-Newton sources in this field are neither stars or clusters, we can assume that most of them are AGNs.

Most of the MIPS 24 µm sources are at intermediate and high redshifts; most being LIRGs and ULIRGs

The bulk of the light at 3.6 and 4.5 µm appears to come from evolved stars in galaxies

The 8.0 and 24 µm light traces the star forming regions in galaxies (which explains the large contribution of the 24 µm selected sample to the 8 µm integral resolved galaxy light)

First Paper - Conclusions

- IRAC detected 419 galaxies in the 4’7 × 4’7 area in the Lockman Hole
- based on colors, most of the detected galaxies are likely to be at intermediate redshifts $0.6 < z < 1.3$, but 25% appear to be at $z > 1.3$
- 30% of the 5.8 μm sources and 50% of the 8.0 μm sources show colors indicating higher redshifts ($z > 1.3$)
- The MIPS population contributes up to 60% in the 8.0 μm band (most of which are starburst galaxies at intermediate redshifts)

Second Paper

- Spitzer Observations of the SCUBA/VLA Sources in the Lockman Hole: Star Formation History of Infrared-Luminous Galaxies
- E. Egami et al.
- Pages 130-136
- Received 2004 April 8; Accepted 2004 May 27

Second Paper - Introduction

- Improved sensitivity and spacial resolution achieved by the Spitzer Space Telescope can help to explore the evolution of infrared-luminous galaxies
- Imaged a 5’ × 5’ area in the Lockman Hole East region with IRAC and MIPS
- The first analysis of SCUBA submillimeter and VLA radio sources based on the new Spitzer data
- Papers 1 and 3 discuss comparisons more closely with IRAC sources and extremely red objects, respectively

Second Paper – Observations and Data Reduction

- Only MIPS observations described here (previous paper covered IRAC observations)
- The large source photometry mode minimized dither step lengths and maximize areal coverage overlap within the MIPS 24 µm field of view
- a) total reduced 24 µm image
- b) three-color image produced from the IRAC 3.6, 8.0, and MIPS 24 µm (circles are the 10 SCUBA sources)

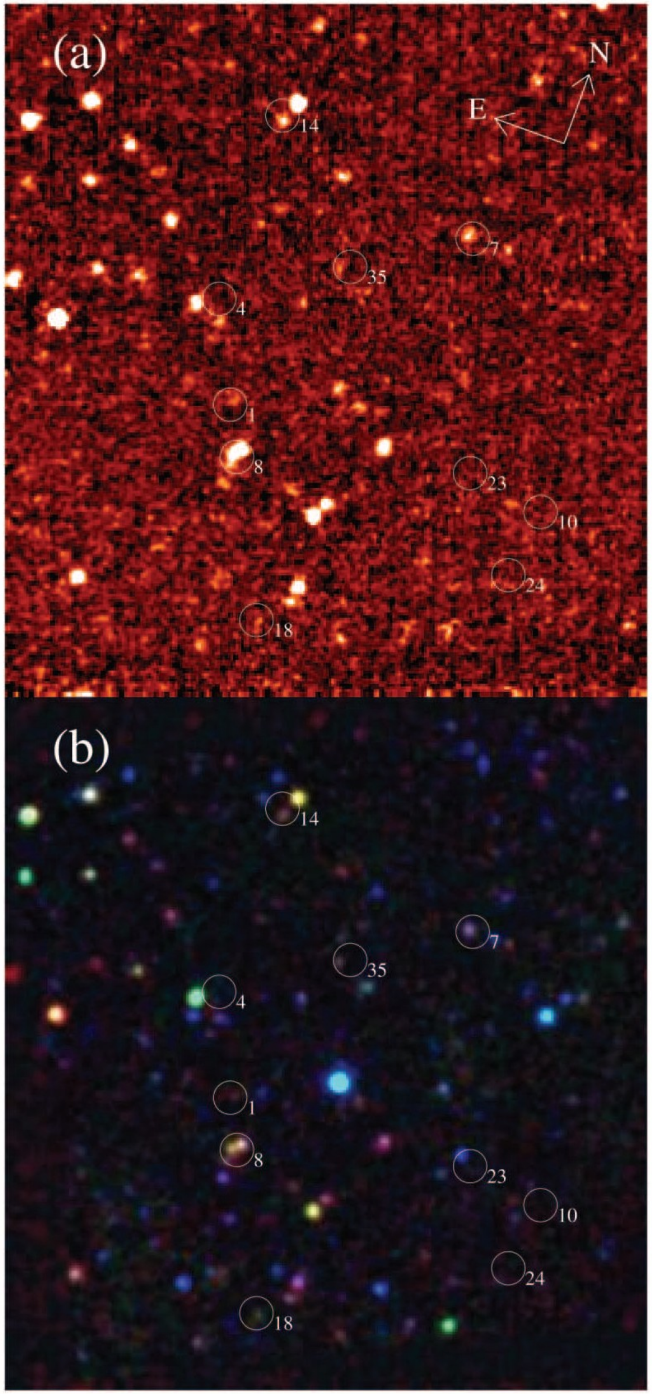

Second Paper – The SCUBA/VLA Sources in the Field

- 10 SCUBA sources in the field imaged by both IRAC and MIPS
- first seven are secure and last three are marginal; depending on whether the signal-to-noise ratio is above or below 3.5
- The field also contains a total of 38 VLA sources above 20 μJy

Second Paper – Identification of SCUBA Sources

- Figure 2 shows *R*-Band images of all 10 SCUBA sources
- IRAC detected the 7 sources with radio detections and MIPS detected 6
- Table 1 shows the IRAC/MIPS flux densities

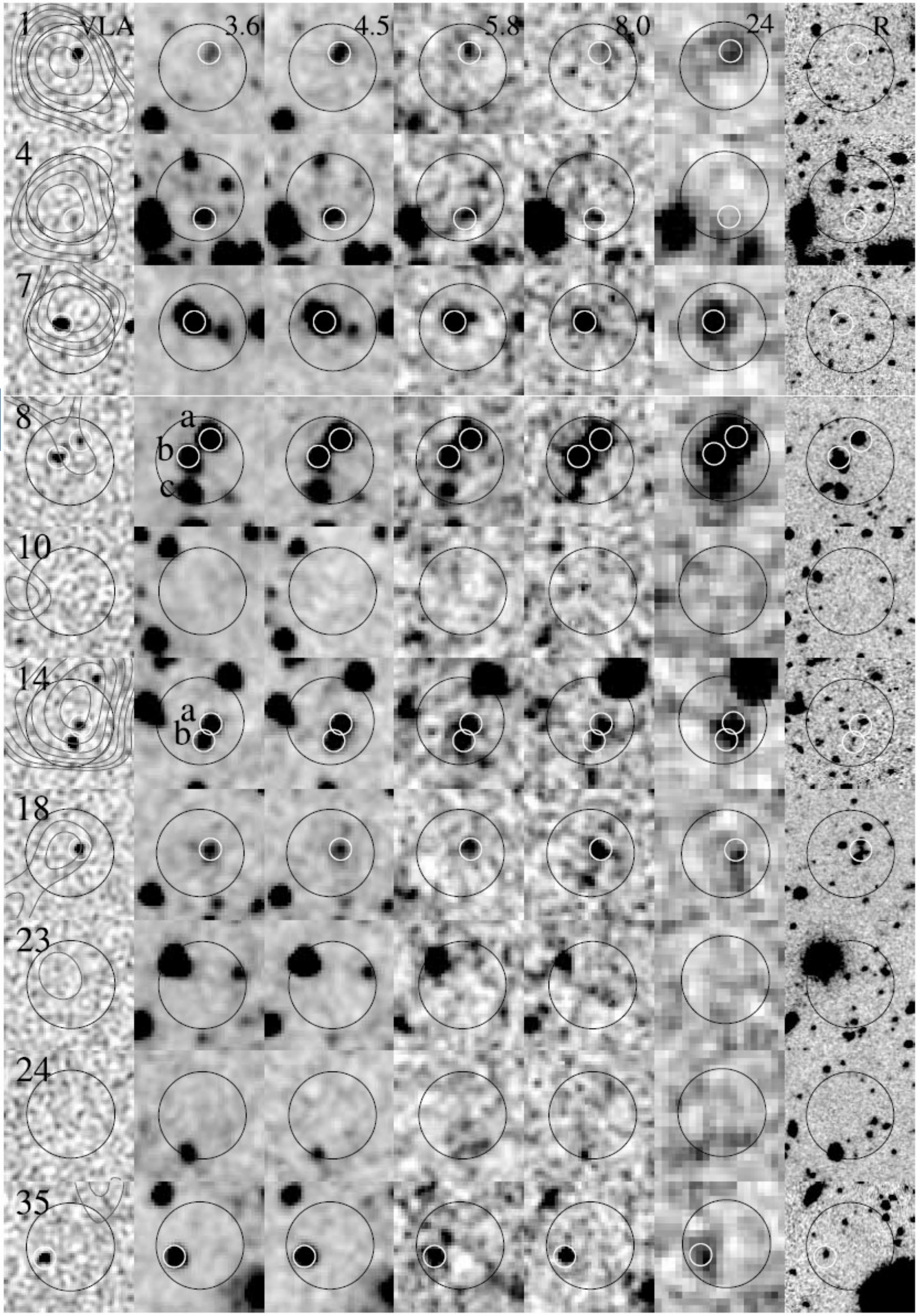

Second Paper – Identification of SCUBA Sources

SCUBA/VLA SOURCES IN THE LOCKMAN HOLE

TABLE 1

Spitzer Flux Measurements of the SCUBA Sources

Source (LE 850)	3.6 μm (μJy)	4.5 μm (μJy)	5.8 μm (μJy)	8.0 μm (μJy)	24 μm (μJy)	850 μm (mJy)	20 cm (μJy)	z_{phot}[a] (Submm/Radio)	z_{spec}[b]	z_{phot} (This Work)	Type
1	3.8 ± 0.6	8.2 ± 1.1	11.8 ± 2.5	10.2 ± 1.7	193 ± 33	10.5 ± 1.6	73 ± 10	$2.6^{+0.4}_{-0.5}$	...	2.6	cold
4	7.7 ± 1.0	10.2 ± 1.4	11.5 ± 2.5	9.6 ± 1.6	...	8.3 ± 1.8	19 ± 8	$4.7^{+1.3}_{-0.5}$	...	2.6	cold
7	65.9 ± 6.9	77.0 ± 8.1	60.1 ± 7.8	52.4 ± 5.9	312 ± 39	8.1 ± 1.9	135 ± 13	$3.6^{+0.4}_{-1.9}$	...	1.8	cold
8b	17.1 ± 2.0	22.3 ± 2.6	37.2 ± 5.3	89.5 ± 9.6	282 ± 59	5.1 ± 1.3	58 ± 12	$3.7^{+1.5}_{-0.7}$	...	~3	warm
8a	72.0 ± 7.5	72.6 ± 7.6	79.0 ± 9.7	112.0 ± 11.9	534 ± 117	...	22 ± 11	...	0.974	...	warm
8c	26.7 ± 3.0	20.7 ± 2.4	17.2 ± 3.1	17.8 ± 2.4	161 ± 47	...	...	...	...	0.9	cold
14b	9.8 ± 1.3	14.7 ± 1.8	22.2 ± 3.7	18.5 ± 2.5	166[c]	6.3[c]	72 ± 12	$2.4^{+1.9}_{-0.4}$	...	2.5	cold
14a	15.2 ± 1.9	20.2 ± 2.4	27.6 ± 4.3	18.6 ± 2.5	83[c]	3.2[c]	36 ± 12	...	2.38	2.5	cold
18	6.1 ± 0.9	5.8 ± 0.9	19.9 ± 3.4	26.4 ± 3.3	125 ± 33	4.5 ± 1.3	47 ± 10	$3.0^{+1.1}_{-1.0}$	2.69	~3	warm
35	23.5 ± 2.7	25.9 ± 2.9	26.3 ± 4.1	34.8 ± 4.2	155 ± 31	6.7 ± 2.3	56 ± 10	...	...	3.0	cold

Notes.—The photometric uncertainties include the 10% calibration errors. The 850 μm fluxes and 20 cm fluxes are from Scott et al. (2002) and Ivison et al. (2002).

[a] Photometric redshifts (le2 type) from Aretxaga et al. (2003).

[b] Spectroscopic redshifts for LE 850.8a (Lehmann et al. 2001), LE 850.14a (R. J. Ivison et al. 2004, in preparation), and LE 850.18 (S. C. Chapman et al. 2004, in preparation).

[c] The measured total flux densities of LE 850.14 at 24 μm (249 ± 39 μJy) and 850 μm (9.5 ± 2.8 mJy) were distributed based on the 20 cm flux density ratio.

Second Paper – Spectral Energy Distribution and Redshifts

- the paper discusses the VLA 20 µJy sample (containing 7 of the 9 SCUBA radio components)
- VLA sample consists of 37 objects; all are detected in the four IRAC bands (29 are detected at 24 µm)
- The SEDs are classified into two types
  - those showing clear near-infrared stellar continuum hump around 1.6 µm; 32 sources, 86%
  - those showing a featureless power-law continuum; 5 sources, 14%

Second Paper – Spectral Energy Distribution and Redshifts

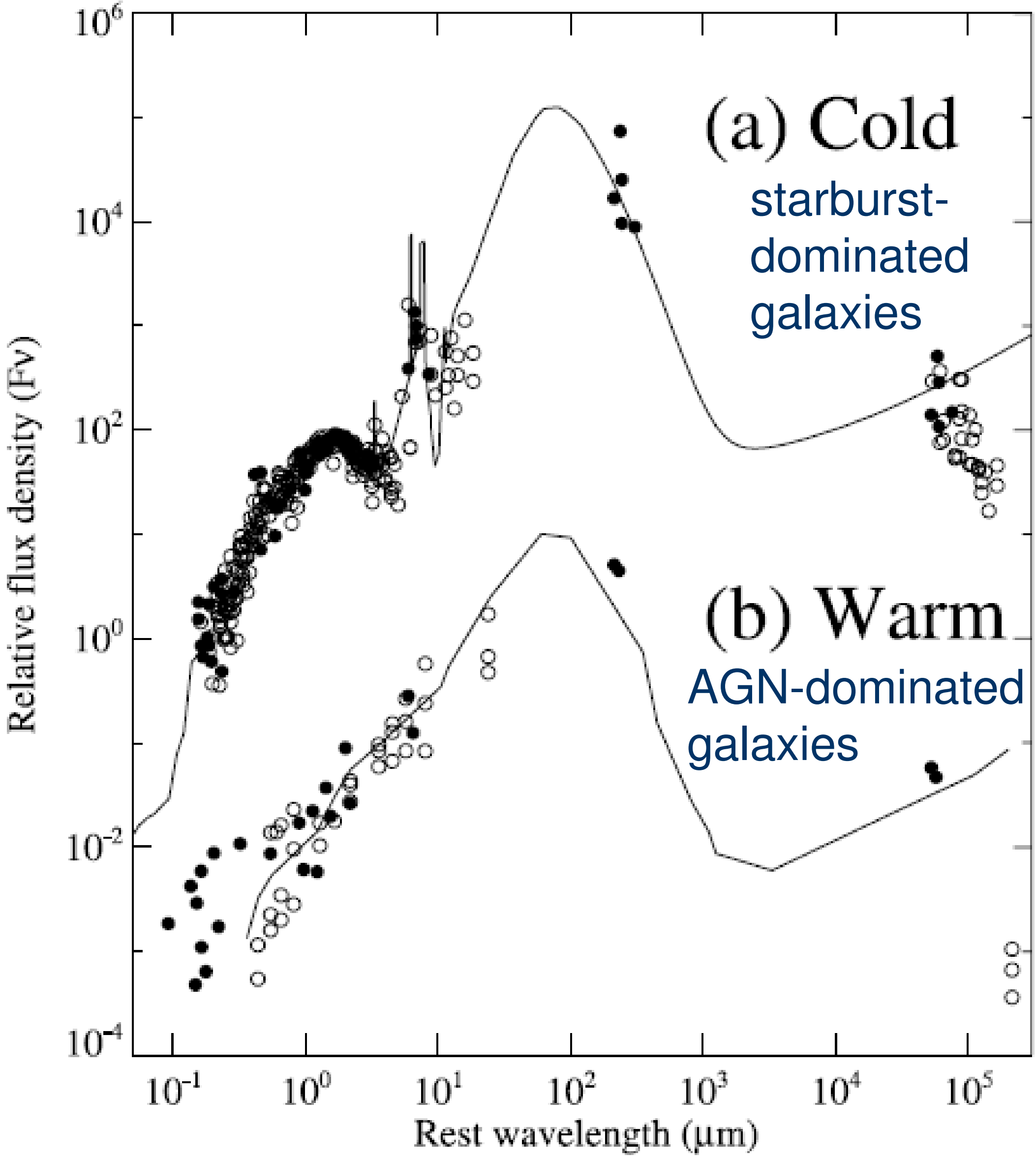

- Figure 3 shows composite SEDs of both types
- The SED of sources with near-infrared continuum hump resembles a “cold” ULIRG SED
  - Small SED dispersion shows accuracy of the photometric redshifts based on the near-infrared continuum hump
- The SED of sources with power law continuum resembles a “warm” ULIRG SED

Second Paper – Spectral Energy Distribution and Redshifts

- Figure 4*a* shows the redshift distribution of the 32 cold sources
  - If we assume that these are starburst-dominated, the figure can be regarded as the redshift distribution of infrared-luminous star-forming galaxies selected in the radio
- Calculated the star formation rate density (SFRD) as a function of redshift (Figure 4*b*)

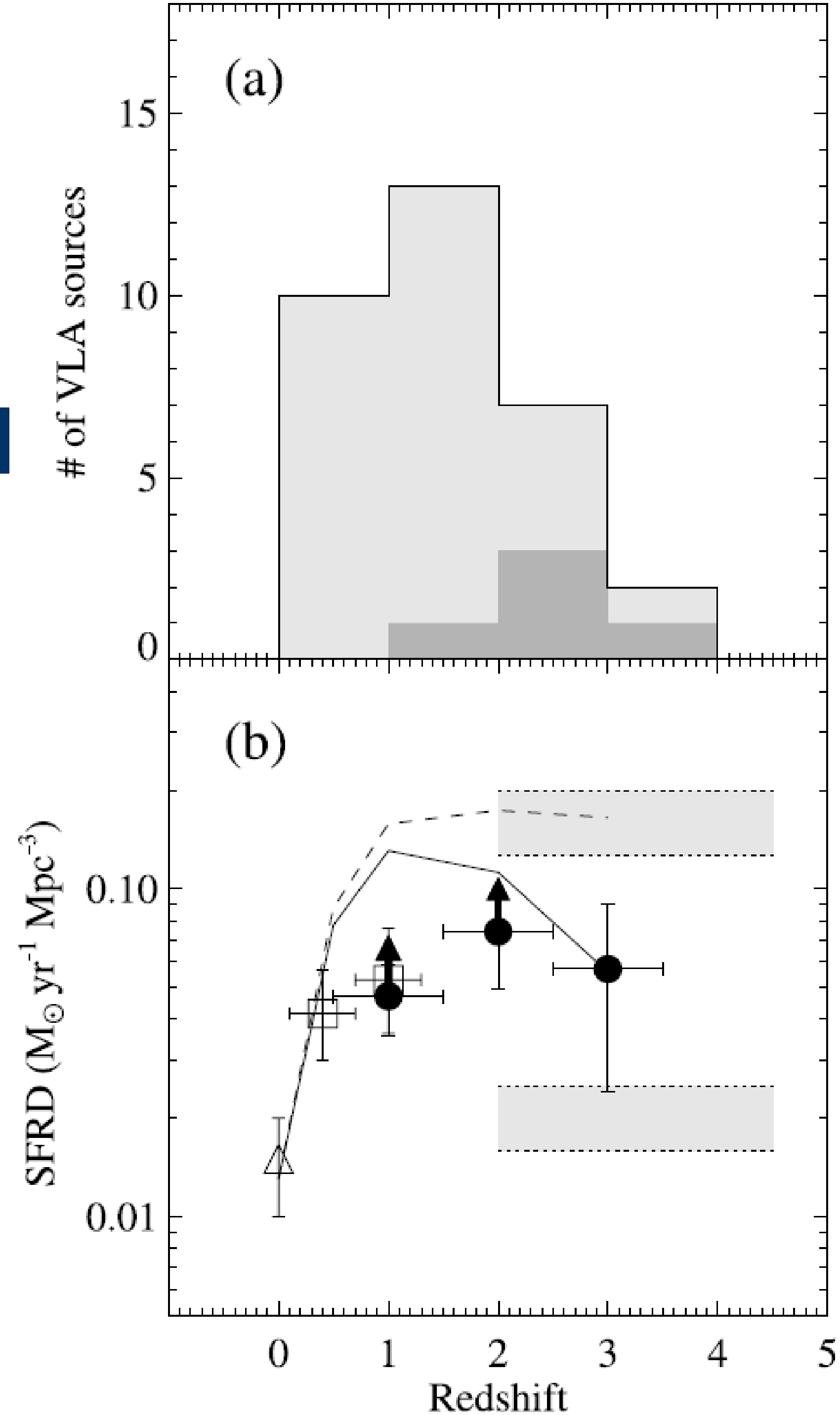

Second Paper – Star Formation History

Using the star formation rate density (SFRD) as a function of redshift:

- A K-correction was applied and it was found that the SFRD at z=1 is close to other authors derived values
- Because the sample contains only the most extreme high-luminosity objects at high redshift, when corrected for dust extinction, the small peak at z=2 still exists (otherwise SFRD stays flat at z=1-3)
  - Therefore, a more substantial completeness correction is still required

Second Paper - Summary

- Nearly all the SCUBA and VLA μJy sources have been detected by Spitzer
- 86% of the sources show similar SEDs well fitted by the SED of a cold ULIRG
  - Using this characteristic, the redshift distribution was derived
  - This allowed for the star formation history to be derived (using radio-infrared correlation)
- These selected galaxies are mostly star-forming (cold) infrared-luminous galaxies at $0.5 < z < 3.5$
  - whose SFRD is probably comparable to that of the optically selected star-forming galaxies

Third Paper

- Extremely Red Objects in the Lockman Hole
- G. Wilson et al.
- Pages 107-111
- Received 2004 March 26; Accepted 2004 May 21

Third Paper - Introduction

- Extremely red objects (EROs) are defined by their very red optical/near-infrared colors
- Faintness makes them difficult to classify (spectroscopically or morphologically)
- The redness implies that these galaxies are either early-type (elliptical and S0) galaxies ($1 < z < 2$), or luminous dusty late-type galaxies at high redshift
- Scientific interest – these two classifications could be the different phases in the formation and evolution of present-day massive elliptical galaxies
- Useful in cosmology because studying their properties (number density, colors, redshift distribution, and star formation rates) can tell crucial constraints on contemporary galaxy evolution models

Third Paper - Introduction

- EROs display extremely strong clustering (supports the theory that they are massive ellipticals)

-BUT-

- Many EROs appear to be highly obscured starburst galaxies
- Morphology studies show that the population consists of an equal mixture of early- and late-type galaxies
- The paper shows how mid-infrared data from the *Spitzer Space Telescope* can easily identify the dusty starburst population

Third Paper – Observations

TABLE 1

FLUX LIMITS

Passband	Galaxies	$(R-[3.6])_{AB}>4.0$	% ERO	$(K-[3.6])_{AB}>0.7$	% ERO	5 σ Mag Limit (AB)
IRAC ch1 3.6 μm	419	64	15.3	70	16.7	23.73
IRAC ch2 4.5 μm	403	64	15.9	70	17.4	23.77
IRAC ch3 5.8 μm	120	50	41.7	48	40.0	21.90
IRAC ch4 8.0 μm	80	35	43.8	46	57.5	21.68
MIPS ch1 24.0 μm	32	11	34.4	13	40.6	18.15

- Observations performed as part of the *Spitzer Space Telescope* Early Release Observation program
- Table 1 shows the number of galaxies detected by Spitzer with S/N>5, and also the corresponding magnitude limits for each passband
  Third Paper - Discussion

Third Paper – Extremely Red Object Selection

TABLE 2
$R-K$ SELECTED ERO SURFACE DENSITIES

Reference	$(R-K)_{AB} > 3.3$; $(R-K)_{Vega} > 5.0$			$(R-K)_{AB} > 3.6$; $(R-K)_{Vega} > 5.3$		
	$K < 21.9$ $(K_{Vega} < 20.0)$	$K < 22.4$ $(K_{Vega} < 20.5)$	$K < 22.9$ $(K_{Vega} < 21.0)$	$K < 21.9$ $(K_{Vega} < 20.0)$	$K < 22.4$ $(K_{Vega} < 20.5)$	$K < 22.9$ $(K_{Vega} < 21.0)$
This work	1.62 ± 0.27 (36)	2.26 ± 0.32 (50)	2.76 ± 0.35 (61)	1.13 ± 0.23 (25)	1.40 ± 0.25 (31)	1.77 ± 0.28 (39)
Cimatti et al. (2002a)	1.50 ± 0.17	...	...	...	...	...
Moustakas et al. (2004)	1.69 ± 0.10	...	...	1.13 ± 0.08	...	...
Roche et al. (2002)	...	...	1.94 ± 0.15	...	...	...
Smail et al. (2002)	...	...	...	...	1.04 ± 0.12	...

- ERO traditionally defined as an object satisfying R – K > 5.0 in the Vega magnitude system
- Table 2 compares their R – K selected sample with published results
  - Note the uncertainties are underestimates because cosmic variance is not included

Third Paper – The R – [3.6] and K – [3.6] Samples

TABLE 3

$R - [3.6]$ SELECTED ERO SAMPLES

z	$(R - [3.6])_{AB} > 4.0$	N	24 μm	%	SCUBA
All		64	11	17.2	4
$0.6 < z < 1.3$	$(K - [3.6])_{AB} > 0$ and $([3.6] - [4.5])_{AB} < 0$	18	2	11.1	0
$z > 1.3$	$(K - [3.6])_{AB} > 0$ and $([3.6] - [4.5])_{AB} > 0$	44	9	20.5	4

- Spitzer color cut that corresponds best with conventional R – K selection is R – [3.6]
- Galaxies with red AB color of R – [3.6] > 4.0 correspond to those with R – K > 3.3
  - Galaxies selected with color R – [3.6] > 4.0 referred as the R – [3.6] selected sample
- 64 objects satisfy the R – [3.6] color cut

Third Paper – The R – [3.6] and K – [3.6] Samples

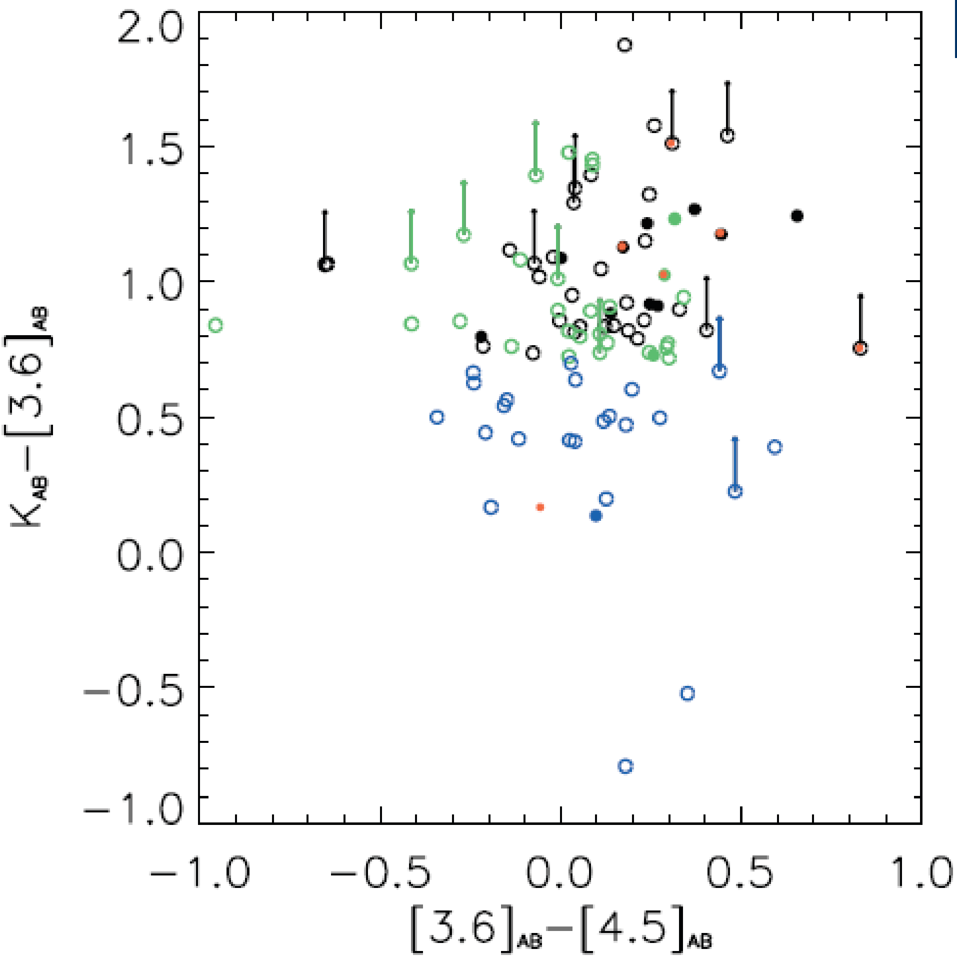

Figure 1 shows a K – [3.6] versus [3.6] – [4.5] color-color diagram

- open and filled blue and **black** circles show the 64 objects selected as EROs on the basis of their red R – [3.6] colors
  - 18 galaxies at (0.6 < z < 1.3)
  - 44 galaxies at (z > 1.3)
- Open and filled green and **black** circles show the 73 objects that satisfied the K – [ee.6] color cut
  - 21 galaxies at (0.6 < z < 1.3)
  - 49 galaxies at (z > 1.3)

Third Paper - Discussion

- There were 40 galaxies in common between the K – [3.6] and R – [3.6] selected samples
- Most of the galaxies selected by both the R – [3.6] and K – [3.6] criteria appear the lie at high redshift
  - Regardless of which color cut used, a high percentage of galaxies detected by IRAC would be classified as extremely red objects

From Table 1: Third Paper – Observations

- 17% of all galaxies detected at 3.6 and 4.6 µm are EROs
- 40% at 5.8 µm and 60% at 8.0 µm
- 40% detected at 24 µm (due to higher background at 24 µm and the relative MIPS/IRAC exposure times

Third Paper - Discussion

- If it is assumed that the correlations between mid and total (8 – 1000 μm) infrared luminosities still apply at higher redshift we can infer the minimum luminosity of a galaxy at any given redshift using the 24 μm flux limit
  Third Paper – Observations
- EROs we select at $0.6 < z < 1.3$ with 24 m detections could be either starbursts or LIRGs
- EROs we select at $z > 1.3$ with 24 m detections could be starbursts, LIRGs, or ULIRGs

Third Paper - Conclusions

- Exploring the nature of EROs with Spitzer (3.6 – 24 μm data)
- Using an R – [3.6] color cut, 64 EROs detected (in 12 minutes of IRAC exposure time)
- Two-thirds of all EROs lie at redshift $z > 1.3$
- The existence of detections at 24 μm allowed lower limits to be placed on the percentage contribution of dusty starbursts to the total ERO population
  - at least 11% of $0.6 < 1.3$ EROs and at least 22% of $z > 1.3$ EROs are dusty star-forming galaxies